ELSEVIER

Journal of Alloys and Compounds 429 (2007) 204–210

Journal of ALLOYS AND COMPOUNDS

www.elsevier.com/locate/jallcom

Milling criteria for the synthesis of nanocrystalline NiAl by mechanical alloying

J. Joardar [a], S.K. Pabi [b], B.S. Murty [c,*]

[a] *School of Materials Science and Engineering, Seoul National University, Seoul 151-742, South Korea*
[b] *Department of Metallurgical and Materials Engineering, Indian Institute of Technology, Kharagpur 721302, India*
[c] *Department of Metallurgical and Materials Engineering, Indian Institute of Technology Madras, Chennai 600036, India*

Received 16 February 2006; received in revised form 20 April 2006; accepted 22 April 2006
Available online 5 June 2006

Abstract

The optimum milling parameters and energy domains for the synthesis of nanocrystalline NiAl by mechanical alloying was determined. The long-range ordered structure of NiAl under various milling conditions was also evaluated. Dominant role of the total energy of the grinding balls over the impact energy of each ball in the phase formation process was observed. A total energy of 200 kJ kg^{-1} was found necessary to trigger the NiAl formation from an equiatomic Ni–Al blend during mechanical alloying in stainless steel as well as in tungsten carbide media. The completion of the reaction required 550 and 700 kJ kg^{-1} of total energy in the stainless steel and tungsten carbide media, respectively. The low-energy requirement for the NiAl synthesis in stainless steel media was attributed to the Fe-contamination during ball milling. A close relation between the enthalpy of formation of the compound and the total energy of the grinding balls for its formation was observed.

Keywords: Mechanical alloying; Ball milling; NiAl; Synthesis; Disordering

1. Introduction

Over the past few decades mechanical alloying (MA) by ball milling has emerged as one of the most versatile solid-state material processing techniques for the non-equilibrium materials such as nanostructured [1–4] and amorphous phases [3,4]. It was demonstrated that the final attainable grain size of nanomaterials by high-energy ball mills [5,6] and conventional low-energy ball mills [7] could be similar. However, wide discrepancies in the phase formation/transformation reactions were observed even with identical composition of the starting blends. For example, ball milling of identical composition of Al–Ti blends under similar conditions in vibratory mill produced amorphous phase or crystalline products with change of grinding ball diameter from 4.8 to 19.1 mm, respectively [8]. Such observation evidence the role played by the various milling parameters in influencing the defect structure and diffusion behavior, which in turn can alter the phase formation/transformation reaction. This has provided a significant impetus to the study of milling dynamics [9–13], computer simulation of ball motion during ball milling [14], milling models [15,16] and milling maps [17,18]. The primary objective of these studies concerns the development of systematic prediction capability for the milling products during ball milling. Most of these early attempts were focused on the crystalline to amorphous phase transformation. The work of Dyck et al. [19] on milling maps for $Ni_3(Si, Ti)$ phase formation correlated the various milling parameters and also demonstrated that the milling time is inversely proportional to the ball-to-powder weight ratio and the cube of milling intensity. Delogu et al. [20] quantified the degree of amorphization in $NiTi_2$ intermetallic, tetragonal-to-monoclinic transition in ZrO_2 and the formation of solid solution in Cu–Ag system as a function of ball-milling time and related the degree of transformation or conversion rates to the impact energy, collision frequency and powder charge.

The synthesis of the Ni–Al phases by MA was studied extensively by several groups [3,21–28]. Many of these studies report B2-NiAl phase formation by a rapid exothermic reaction [18,24]. The present authors could establish that a critical nanocrystallite size of the ball-milled ingredients is a prerequisite for the sudden reaction leading to NiAl formation by a

* Corresponding author.
E-mail address: murty@iitm.ac.in (B.S. Murty).

0925-8388/$ – see front matter © 2006 Elsevier B.V. All rights reserved.
doi:10.1016/j.jallcom.2006.04.045

'discontinuous additive mixing' mechanism [29]. The mechanism was found to change over to a continuous diffusive mode, as observed in the formation of various solid solutions, when high disorder was induced in the NiAl structure by the synergistic effect of Fe-addition (or Fe-contamination from the stainless steel grinding media) and defects generated by severe mechanical deformation involved in the high-energy ball milling [30,31]. Mechanically induced disordering was also reported in other B2 ordered intermetallics, e.g., FeAl [32]. Pochet et al. [32] also underlined the milling conditions for the FeAl disordering during MA. The present work is an attempt to delineate the role of various milling parameters and the energy involved in the process on the formation and disordering of the high temperature congruent melting compound such as NiAl. This is envisaged to provide the necessary conditions for efficient synthesis and disordering of the intermetallic phases by MA.

2. Experimental details

MA experiments were performed in a high-energy planetary ball mill (Fritsch Pulverisette P-5) at milling speeds (disc rotational velocities) of 200, 250 and 300 rpm and different ball-to-powder weight ratio of 5, 10, 15 and 20. However, the number of grinding balls, each of 10 mm diameter, was kept constant at 50, which was found to produce the most optimized energy transfer as evident from Fig. 1. The figure indicates that the ball energy per hit (E_b) as well as the shock frequency (f_b) reaches a saturation level with a minimum of about 50 balls irrespective of the milling speed. As considered in previous work [18], the ball energy per hit, E_b, may be defined by the expression:

$$E_b = 0.5\phi_b m_b {v_b}^2 \quad (1)$$

where m_b and v_b are the mass and velocity of the ball, respectively, while ϕ_b is an efficiency factor related to the filling of the vial, which is close to 1 for one-third filling of the vial [9]. According to Burgio et al. [9] and also Abdellaoui and Gaffet [10], for a single grinding ball in the milling vial of a planetary ball mill, the ball velocity (v_b) is described by the expression:

$$v_b = \frac{2\pi}{60}\left[R_p^2\Omega^2 + (R_v - r_b)^2 w^2 \left\{1 + 2\left(\frac{w}{Q}\right)\right\}\right]^{1/2} \quad (2)$$

where, R_p, R_v and r_b are the radii of the plate, vial and ball, respectively, while w and Ω are the angular velocity of the vial and plate, respectively. The total energy of milling E_t can be expressed as [18]

$$E_t = \frac{E_b n_b f_b t}{W_p} \quad (3)$$

where f_b is the frequency of impacts, t the milling time and W_p is the weight of powder. The frequency of impacts f_b is estimated from the relation [10]:

$$f_b = \frac{60(\Omega - w)n_b}{2\pi} \quad (4)$$

It may be noted that though the expression for the ball velocity (v_b), as derived by Burgio et al. [9] and Abdellaoui and Gaffet [10], considers a single ball motion in a planetary ball mill, the presence of large number of grinding balls in the vial has been incorporated into the expression in the form of the efficiency factor (vial filling factor).

The starting charge contained elemental powder blends of $Ni_{50}Al_{50}$ and $Ni_{40}Al_{40}Fe_{20}$ with particle size of <45 μm (−325 mesh). Tungsten carbide and stainless steel were used as milling media. The milling was carried under toluene bath to avoid oxidation and excessive cold welding. The NiAl phase formation during MA was detected by X-ray diffraction (XRD) analyses using Philips PW1720 diffractometer. The long-range order parameter, S, of NiAl was estimated from the X-ray profiles by comparing the observed ratio of the integrated intensities (I) of 1 0 0 superlattice and 1 1 0 fundamental reflections of the sample with that from the standard JCPDS powder diffraction data files following the expression [33]:

$$S = \sqrt{\frac{\left(\frac{I_{100}}{I_{110}}\right)_{obs}}{\left(\frac{I_{100}}{I_{110}}\right)_{std}}} \quad (5)$$

where "obs" stands for the observed intensity ratio for the sample and "std" stands for that in the JCPDS file. The reordering temperature for the mechanically disordered phase was determined by differential scanning calorimetry (DSC) using Perkin-Elmer DSC7 system.

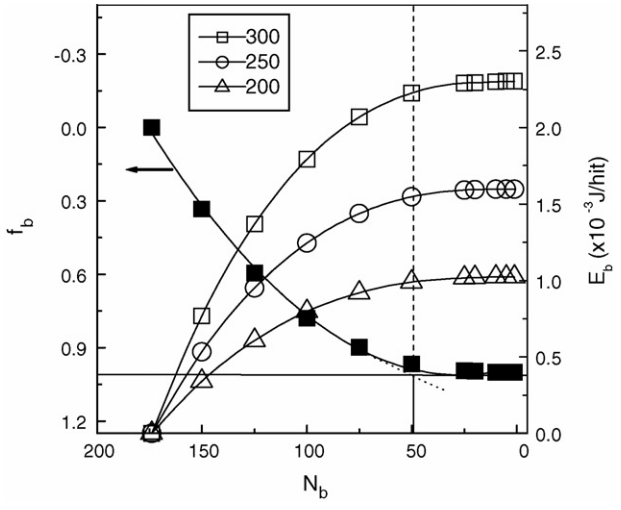

Fig. 1. Variation in shock frequency (f_b) and ball energy (E_b) with number of balls (N_b).

3. Results and discussion

3.1. Formation of nanocrystalline NiAl: parametric phase diagram

Fig. 2 shows the XRD patterns at different milling intervals indicating the formation of nanocrystalline NiAl phase during MA of $Ni_{50}Al_{50}$ elemental blend in tungsten carbide media at a ball-to-powder weight ratio of 10 and milling speed of 300 rpm. The fact that the NiAl formed is nanocrystalline has been confirmed both by X-ray peak profile analysis and transmission electron microscopy [23,29]. Similarly, the nanocrystalline NiAl phase formation was also observed at other milling conditions. The set of these milling conditions for the nanocrystalline NiAl formation in tungsten carbide media were plotted in the form of parametric phase diagram (Fig. 3). As evident from the figure, the formation of NiAl occurs with a ball-to-powder weight ratio of 15 and 20 at a milling speed of 200 rpm, while it forms with even a lower ball-to-powder weight ratio of 10 at a higher milling speed of 250 rpm. At the highest milling speed employed in the present work (300 rpm), NiAl forms at a ball-to-powder weight ratio of 5. Fig. 4 shows the time required for the formation of NiAl under different milling conditions. The results in Fig. 4 reveal that NiAl begins to form at a shorter milling duration and a lower ball-to-powder weight ratio at higher milling speeds. Consequently, the parametric phase diagram shows a gradual change in the slope of the lower boundary delineating the domain of NiAl formation from 0 after 8 h to −10 after 20 h

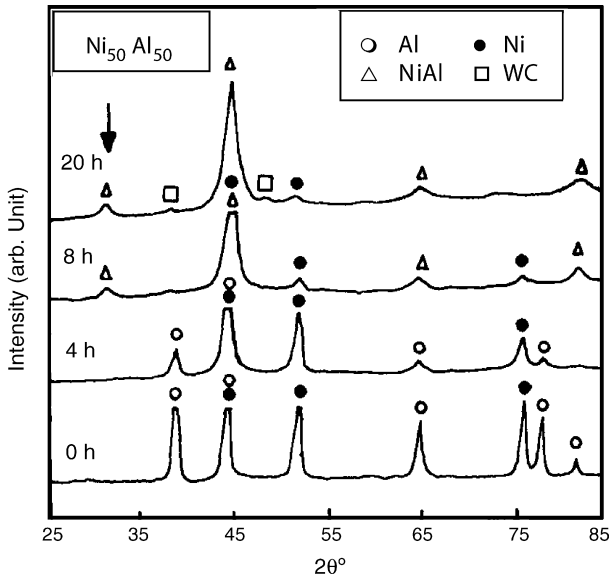

Fig. 2. XRD patterns showing the evolution of nanocrystalline NiAl during MA in $Ni_{50}Al_{50}$ elemental blend milled in tungsten carbide media at 300 rpm and ball-to-powder weight ratio of 10. The NiAl superlattice reflection is shown by the arrow mark.

of milling (Fig. 4). This suggests that NiAl may be generated even at lower energy modes, i.e., a combination of lower milling speed and lower ball-to-powder weight ratio on prolong milling beyond 20 h. Similarly, it also predicts a shorter process times (<8 h) at higher milling speed and ball-to-powder weight ratio.

The long-range order parameter, *S*, of nanocrystalline NiAl after 20 h of MA with tungsten carbide media under different milling conditions are indicated in Fig. 3. Relatively higher *S*-values were observed at lower milling intensities (e.g., 0.7 at 300 rpm and ball-to-powder weight ratio of 5) when compared to the higher intensities (e.g., 0.55 and 0.50 at milling speed of

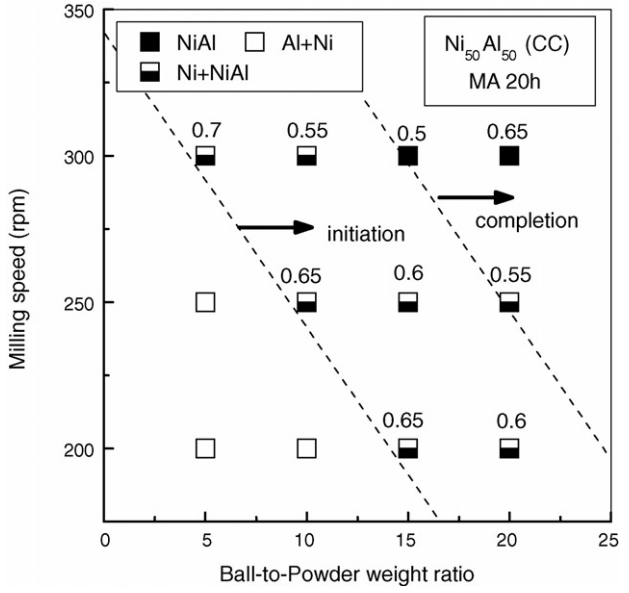

Fig. 3. Parametric phase diagram of NiAl prepared with tungsten carbide media after 20 h of MA. The numbers on the data points refer to the long-range order parameter.

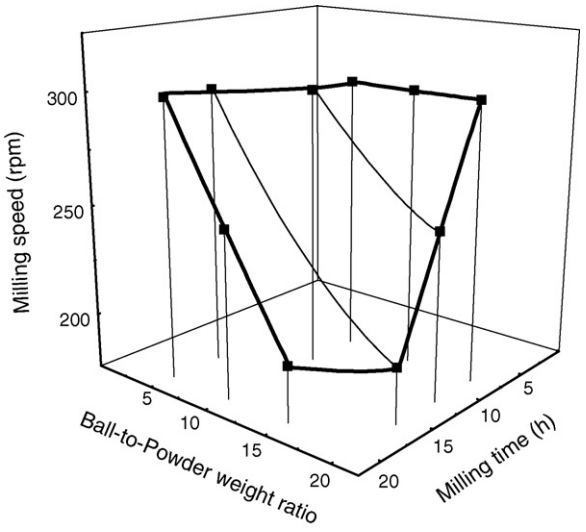

Fig. 4. 3-Dimensional parametric phase diagram with tungsten carbide media indicating the expansion of NiAl domain during MA.

300 rpm and ball-to-powder weight ratio of 10 and 15, respectively). This may be attributed to the lower amount of defects generated during low intensity milling. However, as against such diminishing tendency of *S* with increase in the milling intensity, higher *S* is observed at the highest milling intensity studied in this work (300 rpm at ball-to-powder weight ratio of 20). Such results demonstrate in-situ reordering of the as milled NiAl caused by the temperature generated during MA. The DSC study of the mechanically alloyed powders revealed an exothermic peak between 573 and 773 K (Fig. 5). The peak accounts for the contribution of both grain coarsening and reordering processes as shown in our earlier work [31] and the observed peak temperature is well within the expected temperature rise reported during ball milling, which can typically go up to ~300–873 K [34–36].

Fig. 6 illustrates the set of parameters required for the formation of nanocrystalline NiAl at a given milling speed during MA

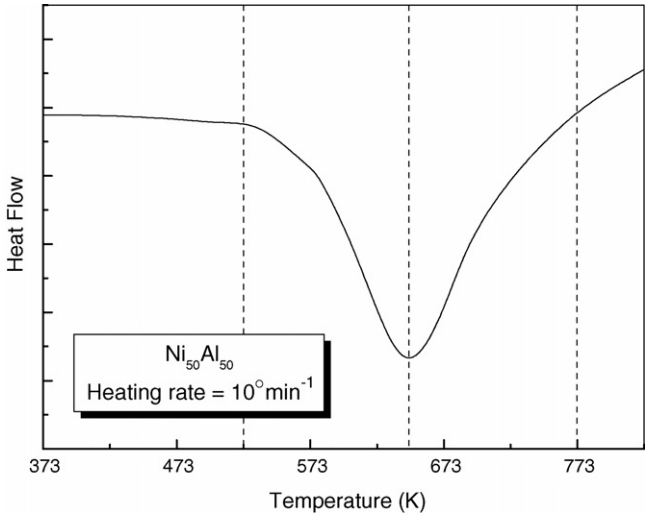

Fig. 5. DSC of NiAl mechanically alloyed for 20 h in tungsten carbide media from equiatomic Ni–Al blend at 300 rpm and ball-to-powder weight ratio of 10.

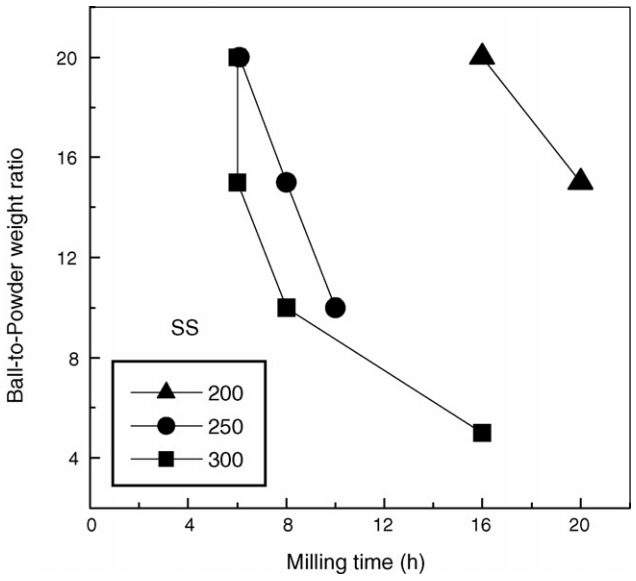

Fig. 6. Parametric phase diagram for NiAl formation during MA with stainless steel media.

with stainless steel grinding media. An increase in the milling speed from 200 to 250 rpm results in a drastic drop in the milling time required for the phase formation. However, further increase in the milling speed up to 300 rpm shows only a marginal reduction in the required milling time. Fig. 6 also shows that the milling conditions with lower ball-to-powder weight ratio of 5 at 250 rpm and with 5 and 10 at 200 rpm were inadequate for initiating the reaction within 20 h of milling. Such observation reflects an inefficient energy transfer below a ball-to-powder weight ratio of 10. It is possible that the NiAl phase formation under such milling conditions may occur on prolong milling as suggested above in the case of tungsten carbide media. It may also be noted that there is a sharp rise in the required milling time for NiAl formation as the ball-to-powder weight ratio drops below 10 at a milling speed of 300 rpm. A similar role of ball-to-powder weight ratio has been reported in earlier work on the amorphization of $Al_{50}Ta_{50}$ alloy [37].

The parametric phase diagram for MA of $Ni_{50}Al_{50}$ in stainless steel media (Fig. 7(a) and (b)) also shows an expansion of the NiAl domain with the increase in milling time as observed in the case of tungsten carbide media. An extremely small amount of NiAl was detected during low intensity milling at 200 rpm and ball-to-powder weight ratio of 15 and 20. It clearly evolves from the parametric phase diagram for nanocrystalline NiAl synthesis with tungsten carbide (Fig. 3) and stainless steel grinding media (Fig. 7(b)) that in spite of the lower intensity milling in the later the conditions are sufficient for the synthesis of NiAl. Such observation may be attributed to the Fe-contamination in the latter, which can induce a solid solution hardening and hence a faster refinement of Ni crystallite size that is likely to assist the nanocrystalline NiAl formation [2].

The extent of disordering of NiAl at different milling conditions with the stainless steel grinding media is indicated in Fig. 7(b). The figure illustrates high degree of disorder at a ball-to-powder weight ratio of 20 at 250 rpm. Such disordered state

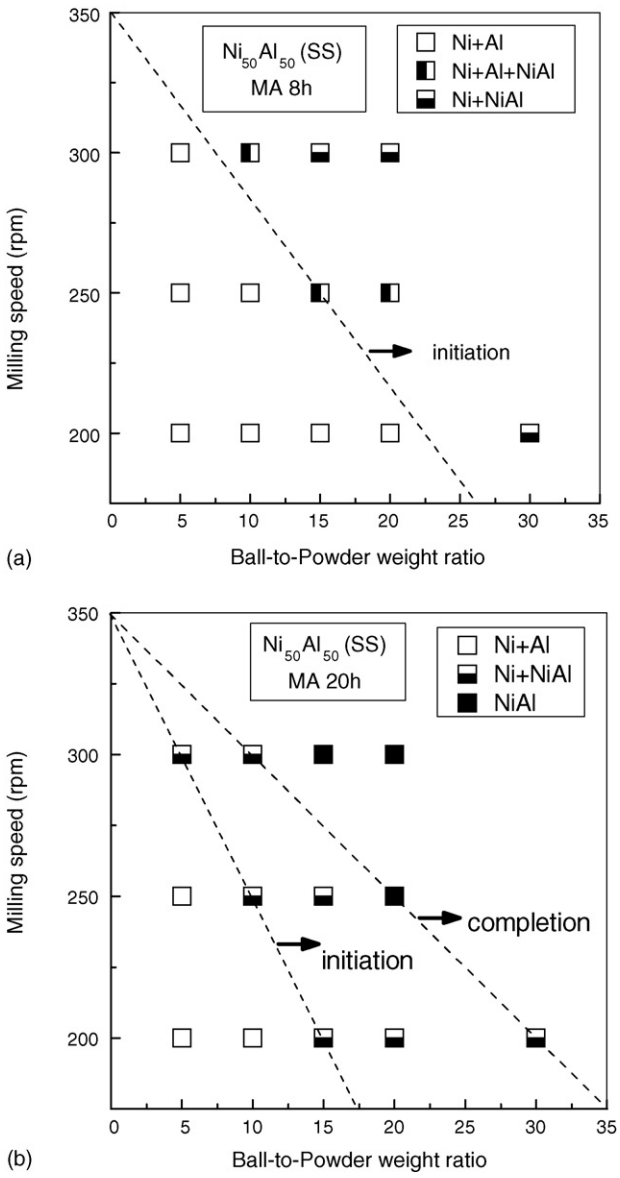

Fig. 7. Parametric phase diagram for NiAl formation after (a) 8 h and (b) 20 h of MA with stainless steel media. Long-range order parameter (S) of NiAl is also indicated in (b).

is achieved at a lower ball-to-powder weight ratio of 10 when the milling speed is raised to 300 rpm, which ensures a higher input of deformation energy.

Fig. 8 shows the formation of nanocrystalline NiAl(Fe) phase during ball milling of the elemental ternary $Ni_{40}Al_{40}Fe_{20}$ blend at different milling parameters. The NiAl(Fe) begins to form at 200 rpm and a ball-to-powder weight ratio of 10. At the higher milling speed of 250 rpm, NiAl(Fe) formation is observed with a lower ball-to-powder weight ratio of 5. The influence of the milling parameters on the S of NiAl(Fe) is also indicated in Fig. 8. It emanates from these results that the formation of NiAl occurs at an even lower milling speed of 200 rpm with a ball-to-powder weight ratio of 15 in case of ternary blend with tungsten carbide media when compared to the binary system in stainless steel media (Figs. 7(b) and 8).

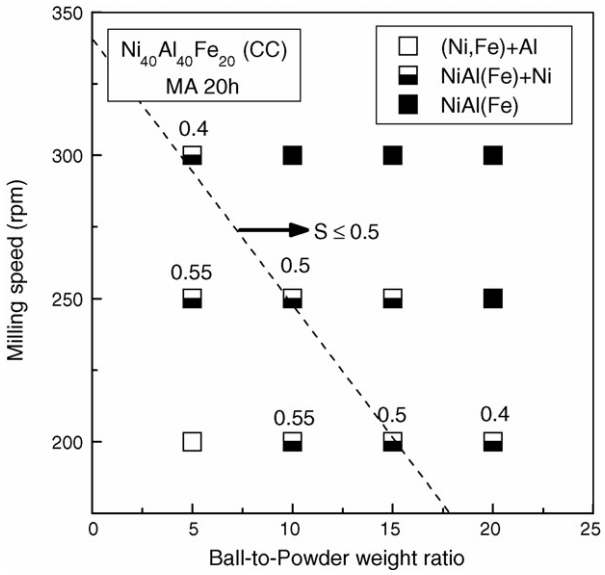

Fig. 8. Parametric phase diagram for NiAl(Fe) formation as well as change in long-range order parameter (S) during MA of ternary blend of $Ni_{40}Al_{40}Fe_{20}$ in tungsten carbide media.

3.2. Energy maps (milling maps)

The basic energy terms for the milling process were examined in order to delineate the energy domains for nanocrystalline NiAl synthesis. The parameters considered in this work include the effective shock energy of the ball per impact (E_b) and the total kinetic energy of the balls (E_t) as expressed by Eqs. (1) and (3). Fig. 9 shows the energy domain for the formation of NiAl in tungsten carbide media. The figure indicates that a total energy, E_t, of ~200 kJ kg^{-1} must be supplied irrespective of the E_b within the studied range of 0.097–0.218 J per hit, in order to trigger the reaction for nanocrystalline NiAl formation. The reaction is complete when a total milling energy of ~700 kJ kg^{-1} is supplied. These results signify the dominant role of E_t over E_b in determining the phase formation process.

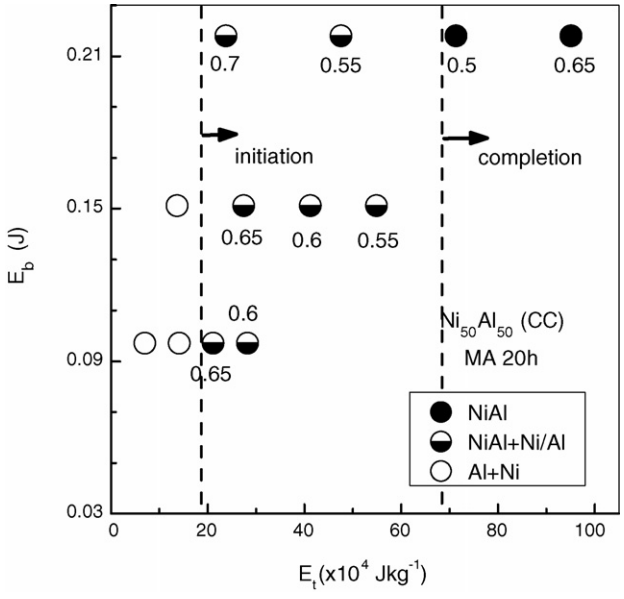

Fig. 9. Milling map for NiAl formation on MA of $Ni_{50}Al_{50}$ with tungsten carbide media along with changes in long-range order parameter (S) at various milling energies.

It is worth noting that the crystallite size of NiAl produced by MA is in the nanocrystalline range. XRD estimation based on single peak analyses by variance method [38] revealed an average crystallite size of ~15 nm from the 211 reflection of the mechanically alloyed equiatomic NiAl in tungsten carbide media. Such nanocrystallite size leads to an excess grain boundary free energy (ΔG_{gb}) in the system given by the expression [39]:

$$\Delta G_{gb} = \frac{3\gamma_{gb} V_m}{d} \quad (6)$$

where γ_{gb} is the grain boundary energy per unit area (may be assumed as ~1000 mJ m^{-2}), V_m the molar volume (~10 cm^3) and d is the grain diameter. The ΔG_{gb} is expected to have a pronounced effect on the overall enthalpy of formation of NiAl for nanocrystallite size. Considering Miedema's model [40] for the enthalpy of formation of equiatomic NiAl and the grain boundary contribution from Eq. (6) for the nanocrystallite size, the overall free energy of formation for the nanocrystalline NiAl is ~28 kJ mol^{-1}. This is of the order of the estimated total energy input of 200 kJ kg^{-1} (~17 kJ mol^{-1} of NiAl) and 700 kJ kg^{-1} (26 kJ mol^{-1} of NiAl). Although, this is only a highly simplified model for the estimation as the actual process also involves substantial amount of energy expended in the generation of heat and disorder in the structure nevertheless, the order of the estimated values matches with the thermodynamic predictions. This indicates that there is a relationship between the enthalpy of formation of the compound and the energy required for its formation. This implies that one need not have to develop a milling map for every compound but possibly can predict the energy required for the formation of the compound from its enthalpy of formation. In fact, a similar correlation between enthalpy of mixing and the energy required for the formation of the phase by ball milling has been observed in case of amorphous phase formation in a number of Zr, Fe and Ti based bulk metallic glass forming compositions very recently [41].

Fig. 9 also shows that the S of NiAl quite expectedly diminishes with the rise in the total energy E_t at a given E_b. For example, S drops from 0.7 at E_t of 235 kJ kg^{-1} to 0.5 at a higher E_t of ~700 kJ kg^{-1}. However, the S shows a rise at the highest E_t of 950 kJ kg^{-1}, which could be due to the temperature build-up during the high-energy ball milling process that might induce simultaneous reordering during milling as discussed earlier.

The energy map for the formation of NiAl during MA of $Ni_{50}Al_{50}$ with stainless steel media is shown in Fig. 10. It is evident from the figure that a minimum E_t of ~200 and ~550 kJ kg^{-1} is essential for the initiation and completion of the NiAl phase formation, respectively. Although the initiation of the phase with tungsten carbide and stainless steel media required same E_t of ~200 kJ kg^{-1}, the completion of the reaction took a relatively lower E_t (550 kJ kg^{-1}) in stainless steel when compared to the tungsten carbide media (700 kJ kg^{-1}). This suggests that the reaction rate is hastened by the rise in Fe-contamination with the progress of milling, which brings

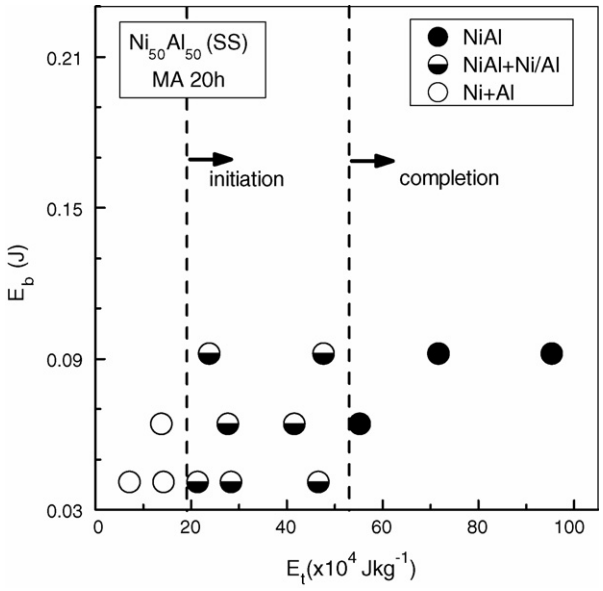

Fig. 10. Milling map for NiAl formation on MA of $Ni_{50}Al_{50}$ with stainless steel media.

down the energy requirements for NiAl formation. At the early stages of milling, the level of Fe-contamination is insignificant and hence the energy required for initiation of the reaction is same in both the media. It may be noted that high amount of Fe-contamination to the extent of 18 at.% was observed during NiAl synthesis in stainless steel media after 20 h of MA at 300 rpm with a ball-to-powder weight ratio of 10 [42]. Similar level of Fe-contamination (∼17 at.%) during mechanical alloying of Cr–Si system in stainless steel media was reported by Fernandes et al. [43].

The present study reveals that MA of the ternary blend leads to the formation of NiAl-rich phase at a very low total energy, $E_t \sim 135\,kJ\,kg^{-1}$ (Fig. 11). The E_t required for the completion

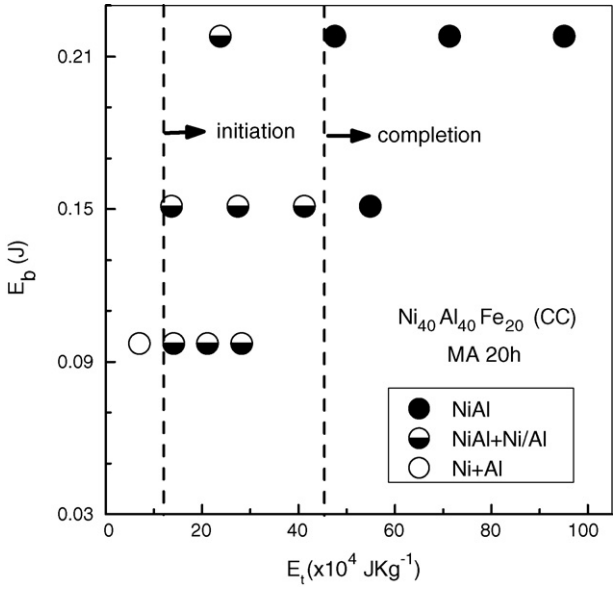

Fig. 11. Milling map for the formation of NiAl(Fe) on MA of $Ni_{40}Al_{40}Fe_{20}$ with tungsten carbide media.

Table 1
E_t for nanocrystalline NiAl formation during MA

Blend composition	Grinding medium	E_t (kJ kg^{-1})	
		Initiation	Completion
$Ni_{50}Al_{50}$	Tungsten carbide	200	700
$Ni_{50}Al_{50}$	Stainless steel	200	550
$Ni_{40}Al_{40}Fe_{20}$	Tungsten carbide	135	450

of the reaction is also lower in the ternary blend (∼450 kJ kg^{-1}) when compared to that in binary blend mechanically alloyed with stainless steel media (∼550 kJ kg^{-1}). A comparative energy data for NiAl formation from binary and the ternary blends ball milled under identical condition is shown in Table 1. The role of Fe in enhancing the reaction kinetics for NiAl synthesis during MA is evident from Table 1. The low-energy requirement for milling with externally added Fe (ternary blend) when compared to the milling of binary blend with stainless steel media appears to be due to the availability of Fe in the early stages of NiAl formation in the former case while in the latter, Fe-contamination becomes significant only on prolong milling.

4. Conclusions

1. The parametric phase diagrams and energy maps for the formation of nanocrystalline NiAl from a binary equiatomic elemental blend during MA with stainless steel as well as tungsten carbide media and ternary $Ni_{40}Al_{40}Fe_{20}$ blend in tungsten carbide media were developed.
2. The NiAl phase formation from binary equiatomic Ni–Al blend required a minimum E_t of ∼200 kJ kg^{-1}. The completion of the process required ∼550 and 700 kJ kg^{-1} in stainless steel and tungsten carbide grinding media, respectively. The values were found to be close to the thermodynamic enthalpy of formation of the equiatomic NiAl considering the contribution of excess grain boundary energy in the nanocrystalline NiAl.
3. The total energy, E_t of 135 kJ kg^{-1} was sufficient for triggering NiAl formation during MA of the ternary $Ni_{40}Al_{40}Fe_{20}$ blend in tungsten carbide media.
4. The enhanced reaction kinetics for the NiAl formation in stainless steel media and also with ternary blend milled in tungsten carbide media was attributed to the presence of Fe in the system.
5. The dominant role of E_t when compared to E_b, in the completion of NiAl phase formation was established.
6. A relation between the enthalpy of formation of the compound and the energy required for its formation during MA has been observed.

References

[1] H. Gleiter, Prog. Mater. Sci. 33 (1989) 223.
[2] E. Hellstern, H.J. Fecht, C. Garland, W.L. Johnson, J. Appl. Phys. 65 (1989) 305.
[3] B.S. Murty, S. Ranganathan, Int. Mater. Rev. 43 (1998) 101.
[4] C. Suryanarayana, Prog. Mater. Sci. 46 (2001) 1.

[5] J. Eckert, J.C. Holzer, C.E. Krill, W.L. Johnson, J. Mater. Res. 7 (1992) 1751.
[6] H.J. Fecht, Z. Metall. 94 (2003) 1134.
[7] D. Oleszak, P.H. Shingu, J. Appl. Phys. 79 (1996) 2975.
[8] Y.H. Park, H. Hashimoto, R. Watanabe, Mater. Sci. Forum 88–90 (1992) 59.
[9] N. Burgio, A. Iasonna, M. Magini, S. Martelli, F. Padella, Il Nuovo Cimento 13 (1991) 459.
[10] M. Abdellaoui, E. Gaffet, Acta Metall. Mater. 43 (1995) 1087.
[11] C. Caravati, F. Delogu, G. Cocco, M. Rustici, Chaos 9 (1999) 219.
[12] P.P. Chattopadhyay, I. Manna, S. Talapatra, S.K. Pabi, Mater. Chem. Phys. 68 (2001) 85.
[13] J. Alkabro, S. Begin-Colin, A. Mocellin, B. Warren, J. Solid-State Chem. 164 (2002) 88.
[14] R. Watanabe, H. Hashimoto, G.G. Lee, Mater. Trans. JIM 36 (1995) 102.
[15] D.R. Maurice, T.H. Courtney, Metall. Trans. 21A (1990) 289.
[16] M. Magini, A. Iasonna, F. Padella, Scripta Metall. 34 (1996) 13.
[17] E. Gaffet, Mater. Sci. Eng. 35A (1991) 291.
[18] B.S. Murty, M. Mohan Rao, S. Ranganathan, Acta Metall. Mater. 43 (1995) 2443.
[19] S.V. Dyck, L. Delaey, L. Froyen, L. Buekenhout, Acta Mater. 46 (1998) 2831.
[20] F. Delogu, C. Deidda, G. Mulas, L. Schiffini, G. Cocco, J. Mater. Sci. 39 (2004) 5121.
[21] M. Atzmon, Phys. Rev. Lett. 64 (1990) 487.
[22] F. Cardellini, G. Mazzone, A. Montone, M.V. Antisari, Acta Metall. Mater. 42 (1994) 2445.
[23] B.S. Murty, K.H.S. Singh, S.K. Pabi, Bull. Mater. Sci. 19 (1996) 565.
[24] T. Chen, J.M. Hampikian, N.N. Thadhani, Acta Mater. 47 (1999) 2567.
[25] C.Y. Chuang, M. Zhu, C.H. Man, Intermetallics 10 (2002) 865.
[26] V.K. Portnoy, A.M. Blinov, I.A. Tomilin, V.N. Kuznetsov, T. Kulik, J. Alloys Compd. 336 (2002) 196.
[27] M.M. Moshskar, M. Mirzaee, Intermetallics 12 (2004) 1361.
[28] J. Guo, X. Du, L. Zhou, Mater. Sci. Forum 475–479 (2005) 749.
[29] S.K. Pabi, B.S. Murty, Mater. Sci. Eng. 214A (1996) 146.
[30] S.K. Pabi, J. Joardar, I. Manna, B.S. Murty, NanoStruct. Mater. 9 (1997) 149.
[31] J. Joardar, S.K. Pabi, H.J. Fecht, B.S. Murty, Philos. Mag. Lett. 82 (2002) 469.
[32] P. Pochet, E. Tominez, L. Chaffron, G. Martin, Phys. Rev. 52B (1995) 4006.
[33] A. Guinier, X-ray Diffraction, Freeman, San Francisco, USA, 1963, p. 259.
[34] C.C. Koch, Int. J. Mechanochem. Mech. Alloy. 1 (1994) 56.
[35] Y.S. Kwon, K.B. Gerasimov, S.K. Yoon, J. Alloys Compd. 346 (2002) 276.
[36] J. Joardar, S.K. Pabi, B.S. Murty, Scripta Mater. 50 (2004) 1199.
[37] M.S. El-Eskandarrany, K. Aoki, H. Itoh, K. Suzuki, J. Less-common Met. 169 (1991) 235.
[38] A.J.C. Wilson, Proc. Phys. Soc. (London) 80 (1962) 20.
[39] A.R. Yavari, Mater. Sci. Eng. A 179–180 (1994) 20.
[40] F.R. deBoer, R. Boom, W.C.M. Matteus, A.R. Miedema, A.K. Niessen, in: F.R. deBoer, D.G. Pettifor (Eds.), Cohession in Metal–Transitional Metal Alloys—Cohession and Structure, vol. 1, North Holland Publication, Amsterdam, Netherlands, 1988.
[41] B.S. Rao, J. Bhatt, B.S. Murty, Mater. Sci. Eng. (in press).
[42] B.S. Murty, J. Joardar, S.K. Pabi, NanoStruct. Mater. 7 (1996) 691.
[43] B.B. Fernandes, G. Rodrigues, G.C. Coelho, A.S. Ramos, Mater. Sci. Eng. A405 (2005) 135.